J Mater Sci (2013) 48:6762–6777
DOI 10.1007/s10853-013-7481-8

The microstructure and fracture performance of styrene–butadiene–methylmethacrylate block copolymer-modified epoxy polymers

H. M. Chong · A. C. Taylor

Received: 4 April 2013 / Accepted: 25 May 2013 / Published online: 11 June 2013

Abstract The microstructure and fracture performance of an anhydride-cured epoxy polymer modified with two poly(styrene)-*b*-1,4-poly(butadiene)-*b*-poly(methyl methacrylate) (SBM) block copolymers were investigated in bulk form, and when used as the matrix material in carbon fibre reinforced composites. The 'E21' SBM block copolymer has a higher butadiene content and molecular weight than the 'E41'. A network of aggregated spherical micelles was observed for the E21 SBM modified epoxy, which became increasingly interconnected as the SBM content was increased. A steady increase in the fracture energy was measured with increasing E21 content, from 96 to 511 J/m^2 for 15 wt% of E21. Well-dispersed 'raspberry'-like SBM particles, with a sphere-on-sphere morphology of a poly(styrene) core covered with poly(butadiene) particles, in an epoxy matrix were obtained for loadings up to 7.5 wt% of E41 SBM. This changed to a partially phase-inverted structure at higher E41 contents, accompanied by a significant jump in the measured fracture energy to 1032 J/m^2 at 15 wt% of E41. The glass transition temperatures remained unchanged with the addition of SBM, indicating a complete phase separation. Electron microscopy and cross polarised transmission optical microscopy revealed localised shear band yielding, debonding and void growth as the main toughening mechanisms. Significant improvements in fracture energy were not observed in the fibre composites, indicating poor toughness transfer from the bulk to the composite. The fibre bridging observed for the unmodified epoxy matrix was reduced due to better fibre–matrix adhesion. The size of the crack tip deformation zone in the composites was restricted by the fibres, hence reducing the measured fracture energy compared to the bulk for the toughest matrix materials.

H. M. Chong · A. C. Taylor (✉)
Department of Mechanical Engineering, Imperial College London, South Kensington Campus, London SW7 2AZ, UK
e-mail: a.c.taylor@imperial.ac.uk

Introduction

Epoxies are highly crosslinked, amorphous thermoset polymers which exhibit very good high-temperature performance, high modulus, high strength and low creep. This makes them attractive as engineering materials for applications such as adhesives and fibre composites. However, the high crosslink density also makes them inherently brittle materials as they are unable to resist crack initiation and propagation effectively, i.e. epoxies have low fracture toughness.

The toughness of epoxies can be improved by introducing a second phase into the bulk material. The most commonly used, and successful, method to improve the fracture toughness of epoxies is to incorporate rubbery particles. These can be pre-formed, such as core–shell rubber (CSR) particles [1, 2], or can form by phase-separation of an initially-soluble rubber during curing, for example, carboxyl-terminated butadiene-acrylonitrile random copolymer (CTBN) [3, 4]. Similarly, thermoplastic-modification may be used, either with pre-formed particles [5, 6] or through phase-separation [7, 8]. Other methods include the addition of rigid particles such as silica nanoparticles [9, 10], glass microparticles [11, 12] or carbon nanotubes [13, 14]. Hollow particles have also been used, either glass particles [15] or microcapsules containing a healing agent [16]. Hybrid materials, containing more than one type of particle, have also been used. Examples include rubber and solid glass microparticles [17], rubber and silica

nanoparticles [18] or carbon nanotubes and silica nanoparticles [19]. Some of these tougheners are known to have significant adverse effects on the viscosity of the resin, when used at concentrations sufficient to achieve a reasonably high toughness. This poses a problem as fibre composite manufacturers are increasingly moving towards infusion processes to reduce costs, and hence a low resin viscosity is required. Even if the toughness of the epoxy is increased in the bulk, this toughness does not necessarily transfer to high composite toughness due to the fibres restricting the crack tip deformation zone [20]. The issues of reduced modulus and agglomeration with certain modifiers are also a concern.

Recently, block copolymers (BCPs) have been shown to increase the fracture toughness through generating complex nanostructures by self-assembly within the epoxy network [21–25]. Strong repulsions between the epoxy miscible and immiscible blocks in an amphiphilic BCP induce nanostructuration to form morphologies such as spherical micelles, worm-like micelles, vesicles [22], 'spheres on spheres' and core–shell structures [26]. These ordered nanostructures are then fixed by the curing process of the epoxy polymer. In this case, nanostructures are preferred as they would offer the significant toughening from rubber particles without imposing a heavy penalty in processing. Most of the early work on block copolymer modification of epoxy polymers has focused on the morphologies and mechanical properties, with less emphasis on the toughening mechanisms brought about by the respective morphologies [27–31]. The most commonly quoted toughening mechanisms observed were rubbery phase cavitation, debonding, plastic void growth and shear yielding with large damage zones [22, 24, 25].

The current study investigates how the modification of an anhydride-cured epoxy polymer using two different poly(styrene)-*b*-1,4-poly(butadiene)-*b*-poly(methyl methacrylate) (SBM) BCP affects the microstructure and mechanical properties. Tensile, compression and fracture tests were undertaken to characterise the properties of the modified epoxy polymers, and microscopy was used to identify the toughening mechanisms involved. The modified epoxies were also used as the matrix material in carbon fibre reinforced polymer (CFRP) composites to investigate how effectively the fracture properties were transferred from the bulk to the composite material.

Experimental

Materials

An anhydride-cured epoxy was used in this study. The epoxy resin used was a standard diglycidyl ether of bisphenol A (DGEBA) with an epoxide equivalent weight (EEW) of 185 g/eq, 'Araldite LY556' supplied by Huntsman, UK. The curing agent was an accelerated methylhexahydrophtalic acid anhydride with an anhydride equivalent weight (AEW) of 170 g/eq, 'Albidur HE600' supplied by Evonik Hanse, Germany, and a stoichiometric amount of curing agent was used. The modifier used was a triblock copolymer of poly(styrene)-*b*-1,4-poly(butadiene)-*b*-poly(methyl methacrylate), i.e. SBM, supplied by Arkema, France, under the trade name Nanostrength. The two different grades of SBM used were 'E21' and 'E41', which were supplied in powder form. Both SBM BCPs have low polarity, but E21 has a higher butadiene content and molecular weight than E41, which makes it softer [32].

For the carbon fibre composites, a ±45° biaxial stitched non-crimp carbon fabric, 'XC305/1270' supplied by Gurit, UK, was used. The fabric has an areal weight of 302 g/m^2, and 1.96 stitches per centimetre [33].

Bulk material

To prepare the bulk material, measured amounts of epoxy resin and BCP were first gently mixed together at room temperature by hand to avoid agglomeration. The mixture was then heated in an oven to 120 °C and stirred at a rate of 90 rpm with a mechanical stirrer for about 4 h until all of the powder has fully dissolved in the resin. The mixture was degassed overnight in a vacuum oven at 60 °C to remove the air bubbles trapped during stirring. The curing agent was added, and stirred thoroughly at 60 °C for 15 min at 200 rpm using a mechanical stirrer. The mixture was then degassed again at 70 °C in the vacuum oven. The resin mixture was poured into pre-heated release agent coated (Frekote 55NC, Henkel, UK) steel moulds to produce bulk polymer plates which were 3 or 6 mm thick. The steel moulds were then placed in a fan oven, and the epoxy was cured at 90 °C for 60 min, followed by a post-cure at 160 °C for 120 min.

CFRP composites

Quasi-isotropic (QI) CFRP panels with unmodified and modified matrices were manufactured using the resin infusion under flexible tooling (RIFT) method. The biaxial stitched non-crimp carbon fabric was used to produce 16 ply composite panels, to give a final thickness of about 5 mm. An insert film of poly(tetrafluoroethylene) (PTFE), about 15-μm thick, was placed in the mid-plane during the lay-up process to initiate the starter crack during the fracture tests. The composite panels were then cured under the same cure conditions as the bulk material. The heat was provided by a hot plate (HP1836URS, Wenesco, USA) from the bottom. Insulation material was used to cover the

top to prevent heat loss. The cured composite panels were inspected by ultrasonic C-Scan to ensure that the laminates were free from defects. The fibre volume fraction of the CFRP laminates was measured from the area fraction of the fibres from micrographs of several polished cross-sections. The average fibre volume fraction was calculated to be 56.9 ± 2.7 %, which is identical to the previous results using the same fibres and lay-up [34].

Rheology

Rheological tests were conducted to measure the change in viscosity of the unmodified and modified epoxy resins with temperature. Test samples obtained from mixed and degassed bulk material were tested using a TA Instruments AR2000EX rheometer. The tests were conducted using 25-mm diameter disposable aluminium parallel-plates at a constant shear rate of 0.25/s and a gap of 1000 μm. A temperature ramp from 25 to 120 °C in 30 min was chosen to allow enough time for the polymer to respond to the changes in temperature.

Microstructure and thermal studies

Atomic force microscopy (AFM) was employed to determine the morphology of the bulk material. A MultiMode scanning probe microscope controlled with a NanoScope IV controller and an 'E' scanner from Veeco, USA, was used. The very smooth surface required for scanning was prepared by planing the samples using a PowerTome XL cryo-microtome from RMC Products, USA, at room temperature. The surface was scanned using a silicon probe with a 5-nm tip at a scan rate of 1 Hz, and height and phase images were obtained.

The glass transition temperature (T_g) of each of the bulk samples were measured using dynamic mechanical analysis (DMA), using a Q800 from TA Instruments, UK. Samples of dimensions 60 × 10 × 3 mm^3 were tested in double cantilever mode at 1 Hz. A temperature range of −100 to 200 °C and a heating rate of 2 °C/min were used. The storage modulus, loss modulus and tan δ were calculated as a function of temperature, where the T_g was defined as the temperature corresponding to the peak tan δ value.

Basic mechanical studies

Uniaxial tensile tests were performed to obtain the Young's modulus and tensile yield stress according to the BS ISO 527 [35] test standard. The tests were performed with dumb-bell shaped test specimens of type 1BA, machined from the bulk plates. A gauge length of 25 mm and a displacement rate of 1 mm/min were used. The tests were performed using an Instron 5584 universal testing machine, and the strain in the gauge length was measured using an Instron 2620-601 dynamic extensometer attached to the sample. The maximum tensile stress and Young's modulus were calculated in accordance with the test standard. At least five samples were tested for each formulation.

Plane strain compression (PSC) tests were conducted to determine the compressive yield stress and failure strain, as described by Williams and Ford [36]. Polished test specimens of size 40 × 40 × 3 mm^3 were loaded in compression between two parallel dies of 12-mm width at a displacement rate of 0.1 mm/min using an Instron 5585H testing machine. The results were then corrected for machine and test rig compliance. At least two samples were tested for each formulation. The true stress, σ_c, was calculated using:

$$\sigma_c = \left(\frac{\sqrt{3}}{2}\right)\sigma_E \quad (1)$$

where σ_E is the engineering stress. The true strain, ε_c, was calculated using:

$$\varepsilon_c = \left(\frac{2}{\sqrt{3}}\right)\ln\left(\frac{B_c}{B}\right) \quad (2)$$

where B_c is the compressed thickness and B is the initial thickness. The von Mises equivalent true yield stress and the fracture strain were then calculated.

The flexural modulus of the CFRP composites was measured using a three point bend method in accordance with ISO 14125 [37]. Composite beams of 300 × 15 × 5 mm^3 machined from the composite plates were tested at a rate of 1 mm/min at a span of 240 mm, using an Instron 5584 universal testing machine. The modulus was calculated as per the standard.

Short beam shear tests were conducted to determine the interlaminar shear strength of the CFRP composites in accordance with ISO 14130 [38]. The test specimens were machined to a size of 50 × 25 × 5 mm^3. These dimensions ensured that the failure mode was by interlaminar shear. The samples were tested at a rate of 1 mm/min and a span of 25 mm, using an Instron 5584 testing machine.

Fracture tests

Single edge notched bending (SENB) tests were conducted to determine the plane-strain fracture toughness (K_{IC}) and fracture energy (G_{IC}) of the bulk materials in accordance with ASTM D5045 [39]. Test specimens with a size of 60 × 12 × 6 mm^3 were machined from the bulk plates, and notched. A liquid nitrogen chilled razor blade was placed in the notch and tapped to generate a sharp crack of length a/w ≈ 0.5. The tests were performed using an

Instron 5584 universal testing machine at a constant displacement rate of 1 mm/min. At least six samples were tested for each formulation. The energy method was used to calculate the fracture energy, and the fracture toughness was calculated using the fracture load [39].

Double cantilever beam (DCB) tests were used to measure the composite mode I fracture energy, G_{IC}(composite), in accordance with BS 7991 [40]. Test specimens of 150 × 20 × 5 mm^3 were machined from the composite panels. Aluminium-alloy load blocks were bonded onto the grit-blasted and degreased CFRP specimens using Araldite 2014 adhesive supplied by Huntsman, UK. The tests were performed using an Instron 5584 universal testing machine at a displacement rate of 1 mm/min. At least six specimens were tested for each formulation. The composite fracture energy was calculated using the corrected beam theory method.

Fractographic studies

A Carl Zeiss Leo 1525 field-emission gun scanning electron microscope (FEGSEM) was used to obtain high-resolution images of the fracture surfaces. The samples were first cut shorter using a Struers Accutom-5 precision cutter equipped with a saw blade. The samples were then sputter-coated with an approximately 5-nm thick layer of chromium to prevent charging. An accelerating voltage of 5 kV was used for the microscopic observation.

A sample of each formulation was loaded as far as the strain softening region in the PSC tests. A cross-section was examined using cross polarised transmission optical microscopy (TOM). The tested samples were first cut using an Accutom-5 precision cutter from Struers, UK, fitted with a diamond-coated blade. Each sample was polished and mounted to a glass microscopy slide using an optically transparent adhesive (Araldite 2020, Huntsman, UK). The samples were then ground down to a thickness of 100 μm, and polished prior to examination.

Results

Overview

The bulk materials are discussed first, considering the rheology of the resins, then the morphology and thermo-mechanical properties of the epoxy polymers. The tensile, compressive and fracture results are presented, and the toughening mechanisms of the modified epoxies are identified using microscopy techniques. The fibre composites are then discussed, considering the morphology and the mechanical properties. Finally, the fracture energies and the toughening mechanisms are presented.

Bulk material

Rheology

The changes in viscosity of the unmodified and modified epoxy resins with temperature are shown in Fig. 1. A general trend of decreasing viscosity with temperature was observed with a logarithmic trend for all the formulations. The viscosity also increases with the increasing block copolymer content. The viscosities of the E41 modified epoxies were found to be lower than the E21 modified epoxies. For example, the addition of 10 wt% of E41 increases the viscosity by almost an order of magnitude, but 10 wt% of E21 increases the viscosity by about a factor of 50. Although, the viscosity is increased by the addition of the BCPs, it is still low enough that the composite panels can be readily manufactured using RIFT. The results of the rheological tests were used to identify the optimum infusion temperatures for manufacture of the CFRP.

Morphology

The AFM phase images show the differences in stiffness on the scanned surface which provide the information about the morphology. Selected images are shown in Fig. 2. The unmodified epoxy appears flat and featureless, as expected for a homogeneous thermoset.

The E21 SBM modified epoxy polymers were optically translucent. The E21 SBM phase separated as a network of aggregated spherical micelles [25], see Fig. 2b. As the amount of E21 is increased, the spherical micelles become increasingly interconnected, see Fig. 2c. Various authors, e.g. [41–43], have observed changes in morphology, into a co-continuous phase, for higher concentrations of thermoplastics in epoxy. As the amount of modifier is increased, the viscosity increases and the rate of phase separation reduces. This lack of mobility prevents the secondary phase separating into individual particles before gelation occurs. The presence of light and dark areas within the second phase suggests that the PS and PB have phase separated to form the spherical micellar structure [25]. The width of the interconnecting sections can be as narrow as 130 nm to as wide as 1 μm, as measured from Fig. 2c.

The AFM phase images of the E41 modified epoxy show well-dispersed SBM particles phase separated with a 'raspberry'-like microstructure [21], see Fig. 2d. This 'sphere-on-sphere' morphology has a polystyrene (PS) core with polybutadiene (PB) particles on the surface which appear as the dark spots (as they are the softer phase, they appear dark in the AFM phase images). All the formulations of E41 were opaque. The mean particle diameter increased linearly from 433 nm for 2.5 wt% of E41, to 1.04 μm for the formulation containing 7.5 wt% of E41.

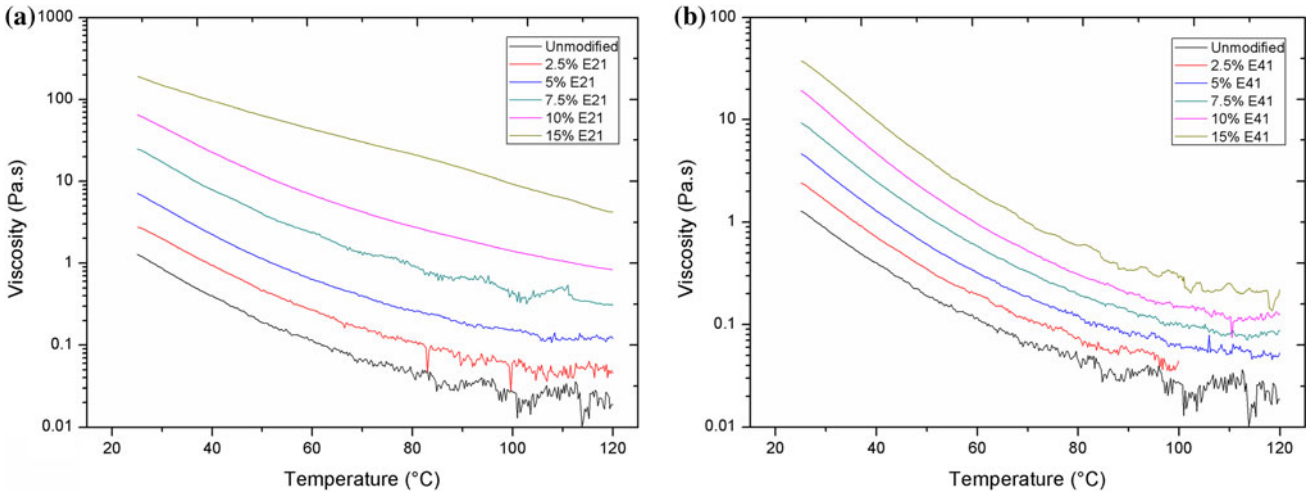

Fig. 1 Viscosity versus temperature plots for (**a**) E21 and (**b**) E41 modified epoxies

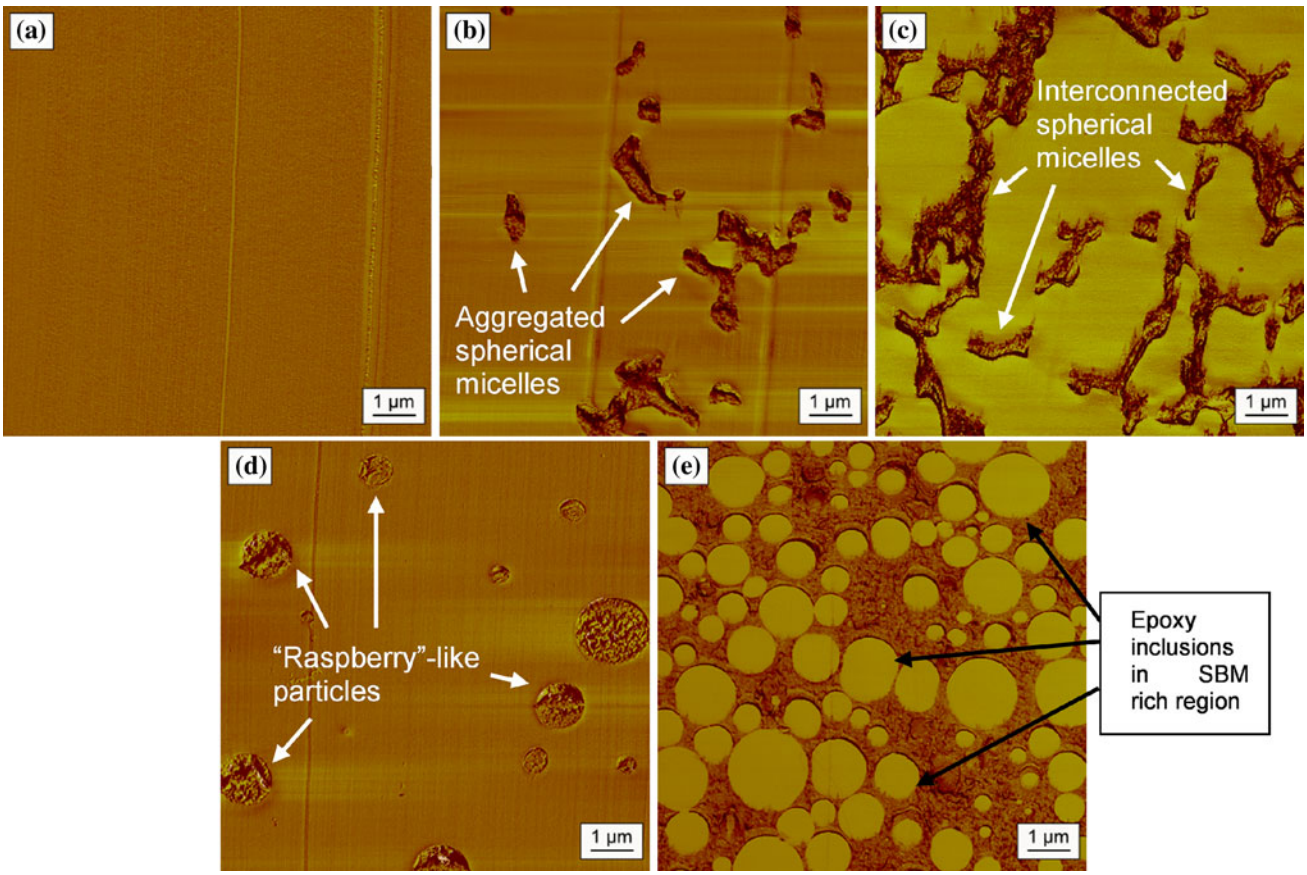

Fig. 2 AFM phase images of (**a**) unmodified, (**b**) 5 wt% E21, (**c**) 10 wt% E21, (**d**) 5 wt% E41 and (**e**) 10 wt% E41 modified epoxy polymer

The use of 10 wt% of E41, and higher concentrations, produced a partially phase-inverted microstructure of epoxy-rich regions with 'raspberry'-like SBM particles, and SBM rich regions with epoxy particles. Figure 2e shows a phase-inverted area with the epoxy particles (lighter areas) within the SBM matrix (darker areas).

Thermomechanical properties

The values of the glass transition temperature, T_g, for the E21 and E41 modified epoxies are summarised in Tables 1 and 2 respectively. The unmodified epoxy has a T_g of 157 °C, in agreement with the literature [34], and the

Table 1 Glass transition temperature, Young's modulus, fracture toughness and fracture energy for E21 modified epoxy

E21	T_g (°C)	E_t (GPa)	K_{IC} (MPa m$^{1/2}$)	G_{IC} (J/m^2)
Unmodified	157 ± 0	2.88 ± 0.06	0.64 ± 0.03	96 ± 9
2.5 wt%	157 ± 1	2.77 ± 0.05	0.79 ± 0.03	167 ± 2
5 wt%	158 ± 0	2.63 ± 0.07	0.98 ± 0.04	290 ± 21
7.5 wt%	158 ± 0	2.50 ± 0.01	1.08 ± 0.05	372 ± 33
10 wt%	157 ± 1	2.41 ± 0.07	1.16 ± 0.03	418 ± 18
15 wt%	160 ± 1	2.04 ± 0.02	1.16 ± 0.02	511 ± 38

Table 2 Glass transition temperature, Young's modulus, fracture toughness and fracture energy for E41 modified epoxy

E41	T_g (°C)	E_t (GPa)	K_{IC} (MPa m$^{1/2}$)	G_{IC} (J/m^2)
Unmodified	157 ± 0	2.88 ± 0.06	0.64 ± 0.03	96 ± 9
2.5 wt%	156 ± 1	2.92 ± 0.06	0.87 ± 0.07	182 ± 22
5 wt%	157 ± 0	2.87 ± 0.07	0.83 ± 0.05	174 ± 13
7.5 wt%	159 ± 1	2.82 ± 0.03	0.89 ± 0.04	219 ± 25
10 wt%	158 ± 1	2.62 ± 0.07	1.66 ± 0.03	637 ± 58
15 wt%	157 ± 1	2.66 ± 0.04	1.67 ± 0.10	1032 ± 27

addition of E21 or E41 does not have a significant effect on the T_g. The position of the peak in tan δ at 157 °C remains unchanged, indicating that complete phase separation occurred.

Figure 3 shows the variation in the storage modulus and tan δ values with temperature. A minor peak was present at −50 °C for all the formulations, and this corresponds to the beta transition temperature of the epoxy, which is associated with localised backbone or side chain motions. The DMA tests also show a very small tan δ peak at −90 °C for the E21 modified epoxies, corresponding to the presence of phase separated PB at high concentrations of E21 due to

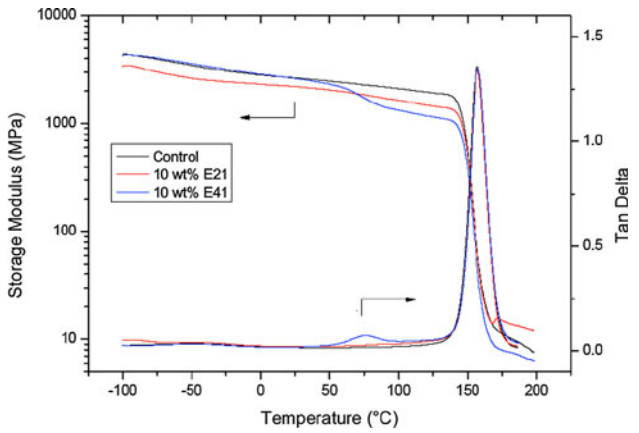

Fig. 3 DMA results for unmodified, 10 wt% E21 and 10 wt% E41 modified epoxies

the higher PB content in E21 than in E41. This peak may be present in the E41 modified epoxies, but it is not a clear peak. The E41 modified epoxies did however have a broad peak at 75 °C which could indicate the phase separation of PS. A similar peak can be seen for the E21 modified epoxies, but it is much smaller due to the relatively lower content of PS. The storage modulus of the E21 formulations was lower than that of the E41 formulations, highlighting the different ratios of the relatively softer PB block in the SBM BCPs.

Tensile and compressive properties

The tensile Young's modulus, E_t, values for the E21 and E41 modified epoxies are summarised in Tables 1 and 2, respectively. The modulus of the unmodified epoxy was measured to be 2.88 GPa, in agreement with the literature [34]. The addition of the relatively soft SBM decreased the modulus of the epoxy as expected. The E21 modified epoxies have a lower modulus than the E41 modified epoxies due to the higher PB content in the E21 block copolymer. The modulus for the E21 modified epoxy decreased linearly with increasing SBM content, to a minimum of 2.04 GPa for 15 wt% of SBM, see Table 1. In contrast, the modulus of the E41 modified formulations is relatively constant at low-BCP concentrations, and there is only a significant decrease in stiffness above 7.5 wt% of E41. This drop corresponds to the change in morphology to a partially phase-inverted microstructure. The presence of the large, relatively soft continuous phase in the epoxy is the cause of this sudden drop in stiffness.

The samples containing E21 at concentrations of 7.5 wt% and above, exhibited extensive stress whitening across their gauge length in the tensile tests, see Fig. 4. The sample stiffness decreased during this stress whitening phase, and then increased again after the entire region had stress whitened. During this stress whitening phase, the particles debond and form voids, which scatter light and cause the white appearance. This debonding occurs before yielding. The stress versus strain trace is non-linear, but the yield point has not been reached in Fig. 4 when fracture occurs. The stiffness before whitening is greater than that after whitening, due to the voids which reduce the stiffness of the sample. The tensile yield stress can be calculated from the PSC data, as described below. For the formulation containing 10 wt% E21, a value of 67 MPa is calculated, so Fig. 4 shows that fracture occurs well before yield.

The compressive modulus, E_c, compressive yield stress, σ_{yc}, true tensile yield stress, σ_{yt}, compressive yield strain, ε_{yc}, failure stress, σ_f, and failure strain, ε_f, values for the E21 and E41 modified epoxies are summarised in Tables 3 and 4 respectively. The trends in compressive modulus were similar to those of the tensile modulus, with the

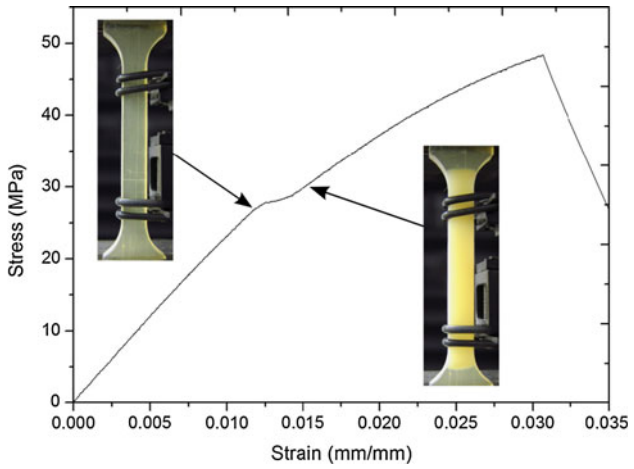

Fig. 4 Extensive stress whitening along gauge length of 10 wt% E21 modified epoxy

compressive modulus of the E21 SBM modified epoxy reducing in a linear manner, while the addition of E41 SBM did not significantly affect the compressive modulus. The absolute values of E_c were typically lower than E_t due to the compliance corrections and frictional effects from the PSC test [36].

The tensile yield stress could not be measured from uniaxial tensile tests due to the brittle nature of the epoxies. However, the constraint in the PSC test and pressure dependence of yielding allows the material to yield in a PSC test [34]. The true tensile yield stress can be calculated from the compressive yield stress obtained from the PSC tests, using the equation:

$$\sigma_{yt} = \sigma_{yc} \frac{\left(3^{1/2} - \mu_m\right)}{\left(3^{1/2} + \mu_m\right)} \tag{3}$$

where μ_m was taken to be 0.2 [44]. The calculated tensile yield stress decreases with the increasing SBM content. The rate of decrease is greater for the E21 modified epoxy than for the E41 modified epoxies, due to the higher PB content of the former and the network structure of the SBM in the epoxy.

The true stress versus true strain plots acquired from the PSC tests show three distinct stages of deformation (see Fig. 5). There is an initial approximately linear elastic region, similar to that from the uniaxial tensile tests, until the yield point. This is followed by a strain softening region where the stress decreases with the increasing strain. It is known that strain softening is a necessary process for localised shear bands to occur [45]. Increasing the strain further results in a strain hardening region where the stress increases more rapidly with strain until the material finally fractures.

Figure 5 shows that the E21 SBM modification suppresses strain softening compared to the unmodified epoxy. This suggests that there is less shear yielding. Figure 6 shows the samples that were loaded to their strain softening limit (i.e. minimum point or positive change in slope after yielding), sectioned, placed between crossed polarisers and examined using transmitted light. The unmodified sample shown in Fig. 6a confirms the evidence of shear band yielding in the compressed region. Highly focused shear bands are clearly visible in the deformed region. As the amount of E21 is increased, the compressed region appears more diffuse, seen as a decrease in the intensity of the shear bands (see Fig. 6b, c). The more diffuse nature could be explained by an increase in the localised shear banding, initiating and terminating at adjacent SBM particles. At 10 wt% E21, the entire compressed region shows diffused shear banding, i.e. more localised shear banding. The E41 modified epoxies show a slight reduction of strain softening and shear yielding behaviour, as shown in Figs. 5 and 6d, e. Figure 6d shows a cross section that is similar to the unmodified epoxy, with a distinct lack of diffuse shear bands. The lack of localised shear banding with the E41 modified epoxies, although not the only toughening mechanism, was consistent with the relatively low fracture energies.

The fracture stress and strain showed no clear trends with increasing SBM content or change in morphology because they are highly sensitive to defects both within and on the surfaces of the sample. Figure 5 shows that cracks form in the samples prior to failure, causing the stress to drop and leading to variability in the measured fracture stress and strain.

Table 3 Compressive modulus, compressive yield stress, calculated tensile yield stress, compressive yield strain, failure stress and failure strain for E21 modified epoxy

E21	E_c (GPa)	σ_{yc} (MPa)	σ_{yt} (MPa)	ε_{yc} (mm/mm)	σ_f (MPa)	ε_f (mm/mm)
Unmodified	1.81 ± 0.15	107 ± 3	85	0.10 ± 0.01	216	0.91
2.5 wt%	1.67 ± 0.02	103 ± 0	82	0.10 ± 0.00	180	0.78
5 wt%	1.63 ± 0.03	97 ± 0	77	0.09 ± 0.00	216	0.88
7.5 wt%	1.54 ± 0.00	91 ± 0	72	0.10 ± 0.00	189	0.90
10 wt%	1.27 ± 0.07	85 ± 2	67	0.12 ± 0.00	224	0.98
15 wt%	1.09 ± 0.05	77 ± 0	61	0.14 ± 0.01	183	0.88

Table 4 Compressive modulus, compressive yield stress, calculated tensile yield stress, compressive yield strain, failure stress and failure strain for E41 modified epoxy

E41	E_c (GPa)	σ_{yc} (MPa)	σ_{yt} (MPa)	σ_{yc} (mm/mm)	σ_f (MPa)	σ_f (mm/mm)
Unmodified	1.81 ± 0.15	107 ± 3	85	0.10 ± 0.01	216	0.91
2.5 wt%	1.65 ± 0.32	105 ± 1	84	0.11 ± 0.02	159	0.87
5 wt%	1.75 ± 0.02	103 ± 0	81	0.10 ± 0.00	225	0.88
7.5 wt%	1.55 ± 0.05	100 ± 0	79	0.11 ± 0.00	189	0.88
10 wt%	1.61 ± 0.06	94 ± 2	75	0.11 ± 0.00	195	0.91
15 wt%	1.76 ± 0.01	93 ± 1	74	0.11 ± 0.00	174	0.88

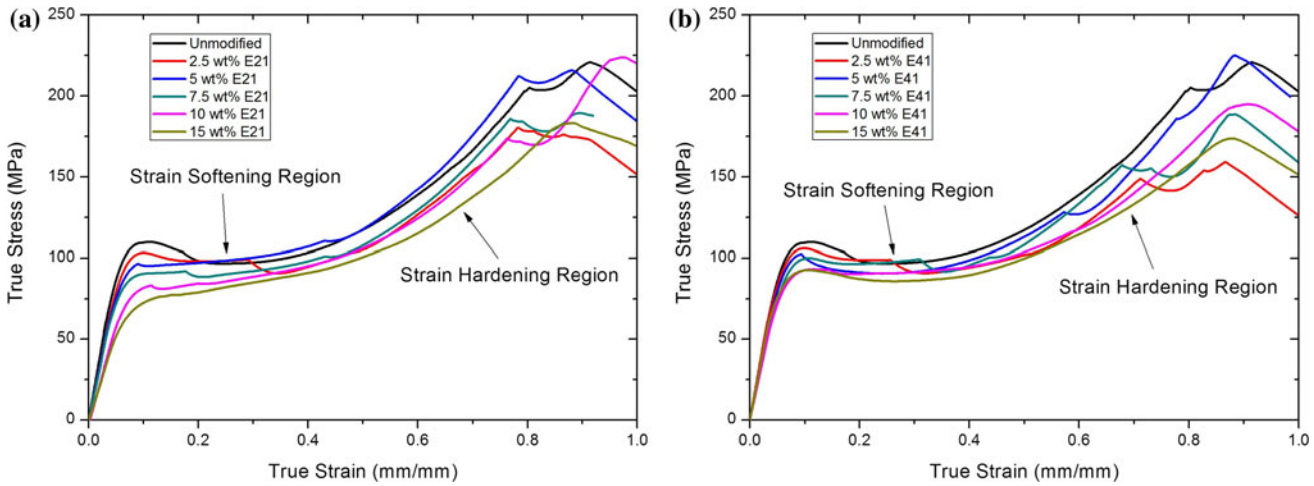

Fig. 5 True stress versus true strain plots for (**a**) E21 and (**b**) E41 modified epoxies

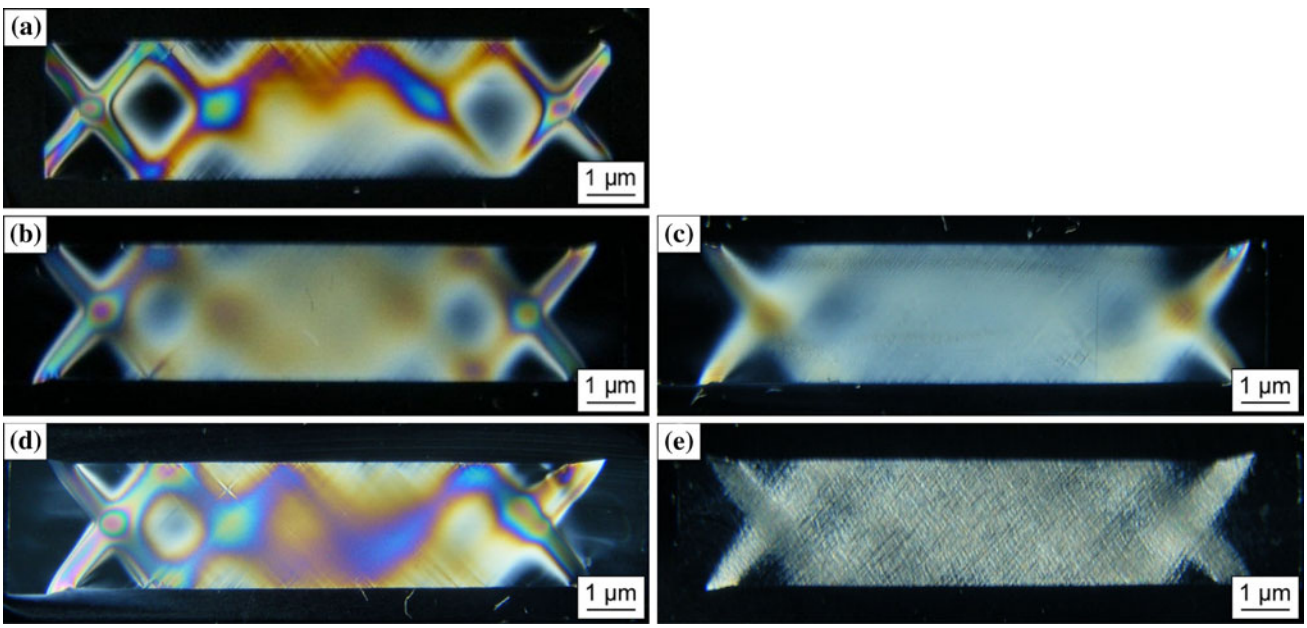

Fig. 6 Cross polarised images of cross section of PSC test samples of (**a**) Unmodified, (**b**) 5 % E21, (**c**) 15 % E21, (**d**) 5 % E41 and (**e**) 15 % E41 modified epoxies

Fracture toughness

The fracture toughness, K_{IC}, and fracture energy, G_{IC}, of the E21 and E41 modified epoxies are summarised in Tables 1 and 2 respectively. The K_{IC} and G_{IC} for the unmodified epoxy were measured as 0.64 MPa $m^{1/2}$ and 106 J/m^2 respectively, in agreement with the literature [34]. The E21 SBM modified epoxies show a linear increase in K_{IC} and G_{IC} to a maximum of 1.16 MPa $m^{1/2}$ and 505 J/m^2 respectively at a loading of 15 wt% (see Fig. 7). This corresponds to an increase of 81 and 376 % in K_{IC} and G_{IC} respectively, which is of the same order as a PB CSR particle modified epoxy [1], see Table 5. The G_{IC} increases as the SBM content is increased from 10 to 15 wt%, whereas K_{IC} does not. This is because the Young's modulus decreases at a higher rate at the higher concentration. While the fracture toughness is slightly below that of a CTBN rubber particle modified epoxy [34], see Table 5, it should be noted that this toughness was achieved without affecting the thermomechanical properties, which was not the case for a CTBN modified epoxy. It is also significantly more effective at toughening epoxy than 20 nm silica nanoparticles [34]. A comparison of the mechanical properties of epoxy modified by various modifiers is shown in Table 5.

The E41 SBM modified epoxies only show a small increase to K_{IC} = 0.89 MPa $m^{1/2}$ and G_{IC} = 222 J/m^2 at 7.5 wt%. However, there is a significant increase to K_{IC} = 1.66 MPa $m^{1/2}$ and G_{IC} = 635 J/m^2 at 10 wt% because of the morphology change to a partially phase-inverted structure (see Fig. 8). The presence of a large, relatively soft phase is more susceptible to yield and would blunt the crack tip, hence, an increase in fracture toughness. The fracture energy increases further at 15 wt% to G_{IC} = 1022 J/m^2.

Hydro and Pearson [25] have reported an increase in K_{IC} of up to 500 % with E20 SBM using a piperidine cured epoxy, which has a lower crosslink density (T_g of 103 °C). They also found that the E40 SBM was less effective at toughening the epoxy than E20 due to the smaller amount of rubbery phase present, as was also found in the current study. E20 has the same chemical composition as E21, but with a lower molecular weight, while E40 has a higher molecular weight compared to E41. The toughening of epoxies is well-known to be dependent on the crosslink density, as Gerard et al. [24] also demonstrated using BCP which increased K_{IC} by about 300 % from 0.76 to 2.96 MPa $m^{1/2}$ for an epoxy system with low crosslink density (T_g of 92 °C). In both the cases, similar BCP

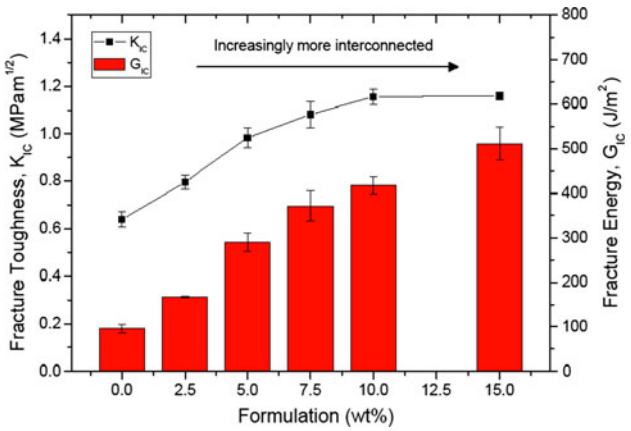

Fig. 7 Fracture toughness, K_{IC}, and fracture energy, G_{IC}, for E21 modified epoxy

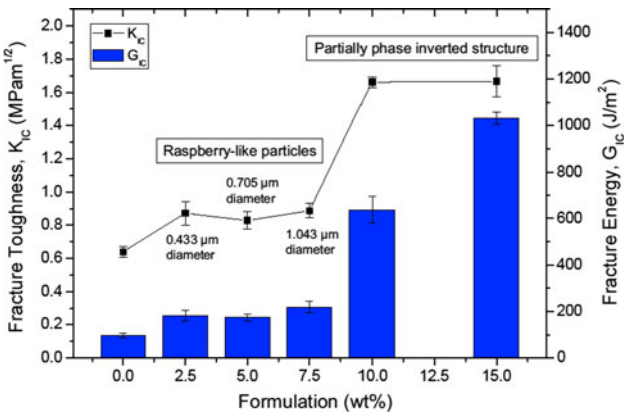

Fig. 8 Fracture toughness, K_{IC}, and fracture energy, G_{IC}, for E41 modified epoxy

Table 5 Comparison between different modifiers in anhydride-cured epoxy, E21 and E41 poly(styrene)-*b*-1,4-poly(butadiene)-*b*-poly (methyl methacrylate) BCP (SBM), poly(methyl methacrylate)-*b*-poly(butylacrylate)-*b*-poly(methyl methacrylate) BCP (MAM), carboxyl-terminated butadiene-acrylonitrile (CTBN), core–shell rubber (CSR) and silica nanoparticles

Modifier	wt%	Effect on T_g	E_t (GPa)	K_{IC} (MPa $m^{1/2}$)	G_{IC} (J/m^2)
E21	10	None	2.41 ± 0.07	1.16 ± 0.03	418 ± 18
E41	10	None	2.62 ± 0.07	1.66 ± 0.03	637 ± 58
MAM [46]	10	Decrease	1.79 ± 0.03	1.22 ± 0.05	407 ± 32
CTBN [34]	9	Decrease	2.35 ± 0.06	1.45 ± 0.20	671 ± 50
CSR [1]	9	None	2.33 ± 0.04	1.31 ± 0.19	485 ± 41
Silica nanoparticle [9]	10	None	3.08 ± 0.06	0.75 ± 0.02	156 ± 8

microstructures were observed. Thompson et al. [47] demonstrated that the increase in fracture toughness of a poly(ethylene oxide)-*b*-poly(ethylene alt-propylene) (PEO-PEP) BCP modified epoxy could be altered from 3 times to 13 times by controlling the molecular weight between crosslinks of the epoxy. Liu et al. [48] concluded that a lower crosslink density increases the capability of an epoxy to be toughened by the elastomeric phase of a BCP. The use of an intermediate crosslink density epoxy system in the current study is the reason for the limited toughness improvement when compared with other studies.

A previous study by Chen and Taylor [46] also showed an increase in fracture toughness when phase inversion was observed in poly(methyl methacrylate)-*b*-poly(butylacrylate)-*b*-poly(methyl methacrylate) (MAM) modified epoxy. In the current study, the amount of E41 added was not enough to cause complete phase inversion. Chen and Taylor showed that when complete phase inversion occurs, the fracture toughness would decrease as the BCP's lack of strength causes premature failure.

Fractographic studies

The fracture surfaces of the unmodified epoxy (see Fig. 9a) appear smooth, and feature only line marks that represent step changes in height as the crack propagates. Crack forking and the multi-planar nature of the surface observed here are the main mechanisms to absorb the excess energy in such brittle materials [49].

The addition of E21 SBM caused the fracture surfaces to appear very rough, with more step changes in the crack plane (see Fig. 9b), indicating more plastic deformation. This behaviour correlates well with the mechanical properties as the yield stress was shown to decrease. The fracture surfaces showed debonded SBM particles, which initiated the void growth around these particles. As the voids in the 5 wt % E21 formulation grew, PB fibrils were formed, which connected the stiffer PS core to the epoxy matrix (see Fig. 9c). It was observed using the FEGSEM that almost all the visible particles exhibited this behaviour. Dean et al. [22] have shown that the formation of drawn fibrils only results from a strong interfacial adhesion by the use of reactive functionalities. The use of nonreactive BCP resulted in a weaker interfacial adhesion and thus would not produce a fibrillar structure. In the current study, as the BCPs have covalent bonding between the blocks, and PB is the central block, fibrils would be expected.

At higher loadings of E21 SBM, the particles become more interconnected to form a network structure (see Fig. 9d, e). Long thin ligaments of the SBM network can be seen around the epoxy matrix, which appears flat and smooth. The fracture surfaces also indicated that at higher concentrations, the SBM becomes a continuous phase where particles of epoxy are surrounded by the SBM-rich phase. The SBM ligaments debonded from the epoxy, and unlike the 5 wt% E21 formulation, there were no fibrils connecting the debonded particles to the epoxy. An interconnected structure reduces the surface area available to form voids, when compared with CTBN modification which forms separate particles, therefore limiting the potential toughening effect. The deformation of the SBM ligaments will absorb energy, increasing the fracture energy with SBM content. However, the toughening effect levels off at 10 wt% of E21 and above as the network is fully interconnected.

The fracture surfaces of the E41 modified epoxy with a loading of up to, and including, 7.5 wt% show that the particles were well dispersed in the epoxy. The particles form a 'raspberry'-like structure with a stiff PS core which is covered with smaller PB particles, see Fig. 10a, as previously observed using AFM. The average particle diameters increased with E41 loading, from 0.76 to 1.22 μm as measured from FEGSEM images. These were slightly larger than the diameters calculated from the AFM phase images. Although, particle cavitation does not occur, some internal damage of the particles can be seen in Fig. 10a. The fracture surfaces also show the debonding of the SBM particles followed by plastic void growth. Particle debonding together with the internal damage of the SBM particles relieves the constraint at the crack tip, hence allowing plastic void growth of the matrix to occur. The difference in the roughness of the fracture surfaces is indicative of their relative fracture toughness values. The fracture surfaces of the E41 modified epoxies appeared much smoother, demonstrating less plastic deformation, and smaller voids were formed. There were also fewer fibrils connecting the particle to the epoxy matrix than for the E21 modified epoxies. This could either be due to the fact that E41 has a lower PB content, hence fewer fibrils, or that there is weak adhesion at the interface. The latter is more likely when considering the relatively low K_{IC} and G_{IC} values. Dean et al. [22] postulated that the presence of fibrils depended on the level of interfacial adhesion, and fibrils appear when the surrounding material deforms plastically.

Partially phase-inverted structures were clearly visible on the fracture surfaces for epoxy samples with 10 wt% and above of E41 (see Fig. 10b). A close up of a particle within the epoxy-rich region (see Fig. 10d) shows the same 'raspberry'-like structure as the lower E41 SBM loadings. The particles in this region were much smaller than at lower concentrations (360-nm diameter for 10 wt%, compared to 820-nm diameter for 5 wt%). The epoxy-rich regions can be viewed as areas with lower loadings of E41, hence the smaller particles. The size of the epoxy particles within the SBM rich regions measured from the fracture surface (740-nm diameter) correlates well with the sizes

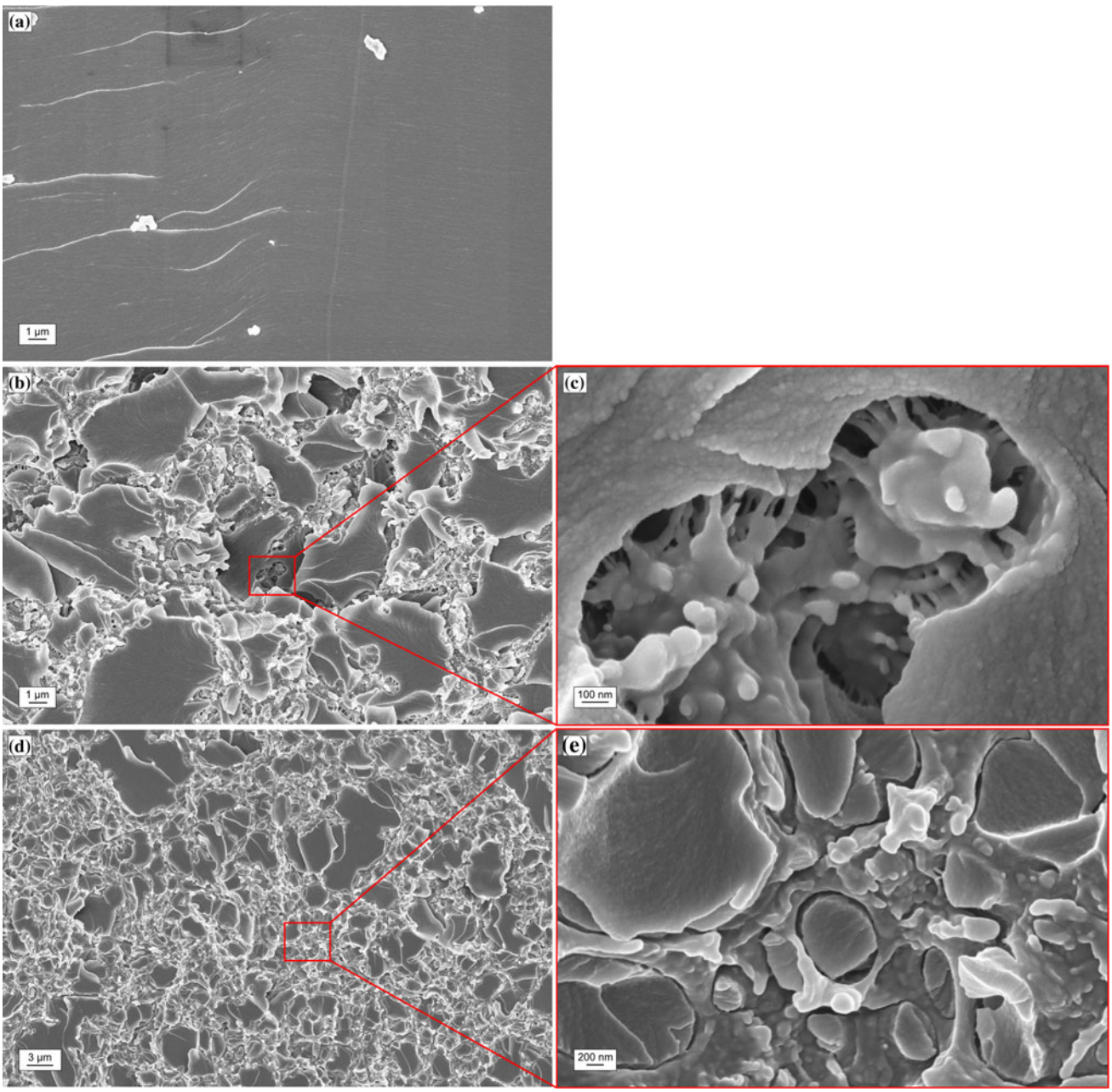

Fig. 9 Scanning electron micrographs of fracture surfaces of epoxy polymers: (**a**) unmodified, (**b**) 5 wt% E21, (**c**) Close up of 5 wt% E21, (**d**) 10 wt% E21 and (**e**) Close up of 10 wt% E21 modified epoxy (Crack propagation direction from *right* to *left*)

calculated from the AFM images (712-nm diameter) which suggest that there was no significant plastic deformation of the epoxy in the SBM rich region as expected. Both epoxy and SBM particles were well dispersed within their respective matrices. In such a partially phase-inverted structure, the relatively soft SBM phase is able to deform much more easily than the epoxy phase and the plastic deformation provides the toughness. The boundary between the SBM rich regions and epoxy-rich regions showed complete debonding at the interface, which suggests weak adhesion between the two phases. Weak adhesion was observed in the lower loadings as well and explains the limited toughening effect as the transfer of stress through the structure would be less.

Carbon fibre composites

As the bulk E41 modified epoxies did not demonstrate much toughening effect, only the E21 SBM was used as the epoxy matrix modifier for the fibre composites.

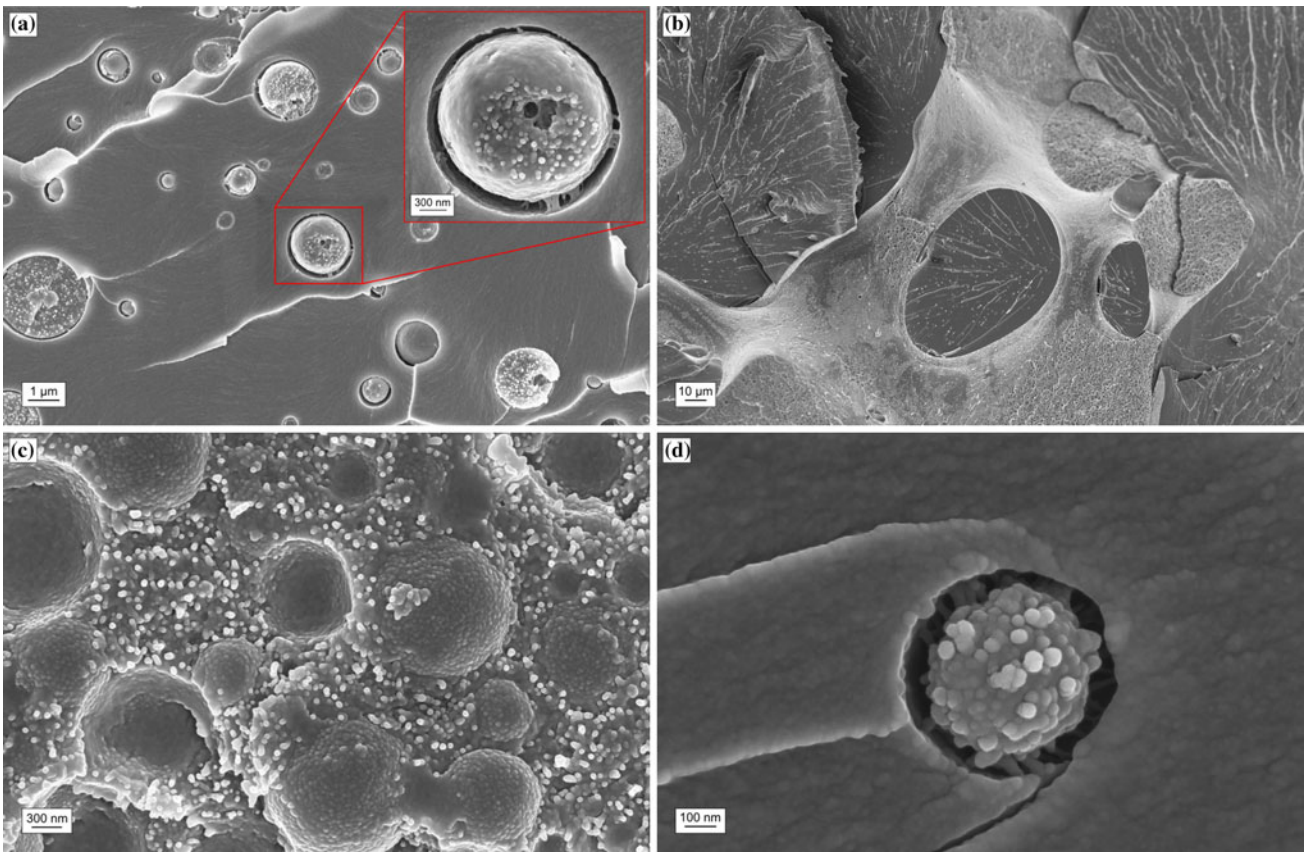

Fig. 10 Scanning electron micrographs of fracture surfaces of epoxy polymers: (**a**) 5 wt% E41, (**b**) 10 wt% E41, (**c**) Close up of 10 wt% E41 in SBM rich region and (**d**) Close up of 10 wt% E41 in epoxy-rich region, modified epoxy (Crack propagation direction from *right* to *left*)

Morphology

Selected backscattered electron micrographs are shown in Fig. 11 to show the morphologies of the composites. Each fibre appears to be well wetted by the matrix, and the fibres are well dispersed. Apart from some defects at the interface between the fibre and matrix due to the fibre damage from polishing, there were no visible voids on the polished cross-sections, even with 10 wt% of E21 added to the epoxy matrix. This shows that there is excellent consolidation of the fibre preforms by the resin. Unlike the particulate modification with micron-sized particles, there was no filtering of the modifiers by the fibres as the SBM was initially dissolved, and then phase separated during curing (i.e. after infusion). This is an advantage as even the smallest gaps between very closely packed fibres can contain toughening particles and hence these regions will not be compromised by lacking a toughened matrix. This is essential for preventing microcracking. The average fibre volume fraction of the CFRP laminates was measured from the polished cross-sections, and was calculated to be 56.9 ± 2.7 %. There was no significant variation among the different formulations used.

Mechanical properties

The measured values of interlaminar shear strength, τ_{SBS}, flexural modulus, E_f, and mode I interlaminar fracture energy, G_{IC} (composite) for the E21 modified CFRP are summarised in Table 6. The flexural modulus remains unchanged with the increasing concentration of E21, as expected as the flexural modulus is strongly dependent on the fibre volume fraction [50] and the fibre volume fraction is constant. The consistent flexural modulus confirms that the laminates were manufactured to a consistent quality with regards to fibre volume fraction, see Fig. 11. A decrease in the interlaminar shear strength is observed, see Table 6, which results from a reduction of matrix modulus with the addition of SBM. The increasing mismatch in stiffness between fibre and matrix with added SBM reduces the compression strength of a composite [51].

Fracture toughness

The unmodified CFRP composite has a mean propagation fracture energy of 303 J/m^2. This is an increase of 216 % compared to the bulk material, which can be attributed to the

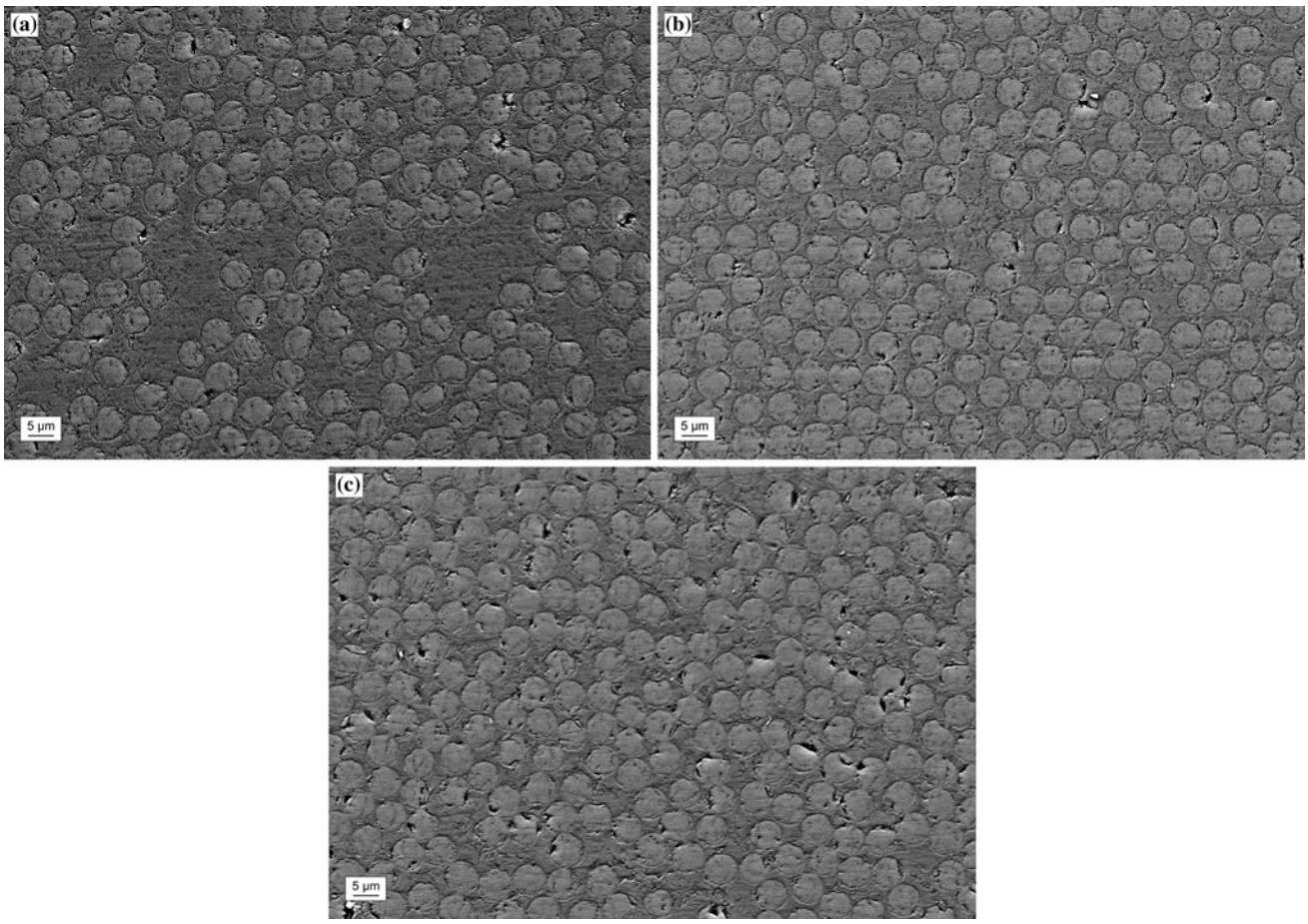

Fig. 11 Backscattered electron micrograph showing cross-section for (**a**) unmodified, (**b**) 5 wt% E21 and (**c**) 10 wt% E21 modified CFRP

Table 6 Interlaminar shear strength, flexural modulus and propagation fracture energy for E21 modified CFRP

E21	τ_{SBS} (MPa)	E_f (GPa)	G_{IC}(composite) (J/m^2)
Unmodified	40.1 ± 1.1	26.8 ± 0.5	303 ± 12
2.5 wt%	42.0 ± 1.1	28.6 ± 1.0	430 ± 9
5 wt%	38.3 ± 0.2	28.0 ± 0.6	394 ± 24
7.5 wt%	30.4 ± 1.0	27.2 ± 1.9	376 ± 15
10 wt%	27.3 ± 1.2	28.3 ± 0.6	312 ± 10

additional fibre pullout and bridging toughening mechanisms in the composite. The maximum G_{IC}(composite) for propagation was measured using 2.5 wt% of E21, and resulted in an increase from 303 to 430 J/m^2. Further addition of E21 resulted in a decrease in the fracture energy. This decrease is partly due to a reduction in the amount of fibre bridging. Figure 12 can be used to compare the amount of fibre bridging by comparing the relative difference between the initiation and propagation fracture energy values, also known as the 'R-curve'. The R-curves are relatively small, and the amount of fibre bridging decreases as the amount of E21 SBM is increased.

The increase in toughness of the bulk epoxy polymer from the addition of E21 SBM was not transferred to give a significant increase in interlaminar fracture energy for the CFRP. The composite fracture energies may be compared to the bulk material values, see Fig. 12. The initiation values of G_{IC}(composite) show no significant change even though the fracture energy of the bulk material, and hence of the composite matrix, is linearly increasing.

This can be explained by considering the plane strain plastic zone radius (r_{pz}) for the bulk materials, which can be calculated using the Irwin model [52]. From Fig. 12, it is clear that the plastic zone sizes at higher concentrations are large in comparison with the inter-fibre distances, which are in the order of 10 μm. This means that the plastic zone will be inhibited from growing by the presence of the stiff fibres and explains the discrepancy between the CFRP initiation and bulk fracture energies [20, 53]. Hunston et al. [20] showed that brittle polymers with G_{IC} values less than 200 J/m^2 benefit the most from fibre reinforcement. In their tests, the tough matrices had incomplete transfer of toughness attributed to the crack tip deformation zone restricted by the closely packed fibres. The transition

between the two behaviours occurs approximately at the point where the deformation zone is equal to the inter-fibre spacing. Similar behaviour was observed in the present study, where the interlaminar fracture energy was lower than the bulk G_{IC} when the plastic zone size was above the inter-fibre spacing. Plastic deformation will also be limited by the fact that the fibres are significantly stiffer than the matrix, hence constraining the crack tip deformation zone [54].

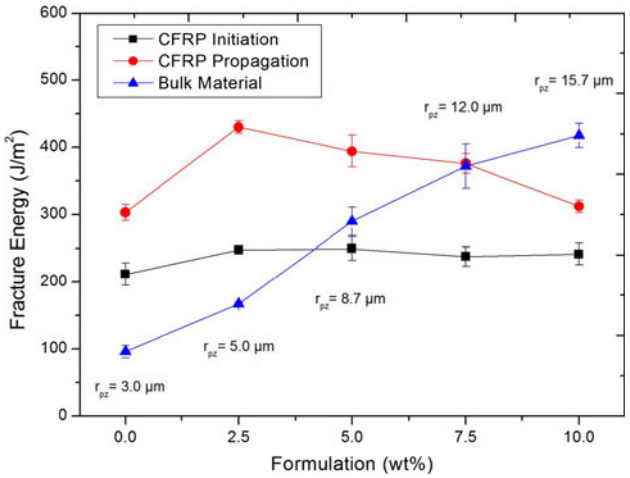

Fig. 12 Propagation G_{IC} and initiation G_{IC} for E21 modified CFRP, showing plastic zone radius (r_{pz}) calculated using the Irwin model for the bulk materials

Quaresimin and Varley [55] attributed poor fracture performance for their E20 SBM modified CFRP composites to the quality of the laminate. They observed a significant number of voids, presumably caused by the entrapment of solvent as the viscosity were increased by the presence of SBM. They also noticed that the SBM phase separated into micron-sized particles instead of nanostructures. However, such effects were not observed in the present study.

Fractographic studies

The fracture surface of the unmodified CFRP (see Fig. 13a) shows a relatively clean fibre surface, indicating an interfacial failure resulting from poor fibre–matrix adhesion. The appearance of the epoxy matrix between the individual fibres was similar to the bulk unmodified epoxy. River lines and step changes in the crack level were visible throughout the entire specimen. The weak interfacial adhesion also explains the fibre bridging and pullout observed during the

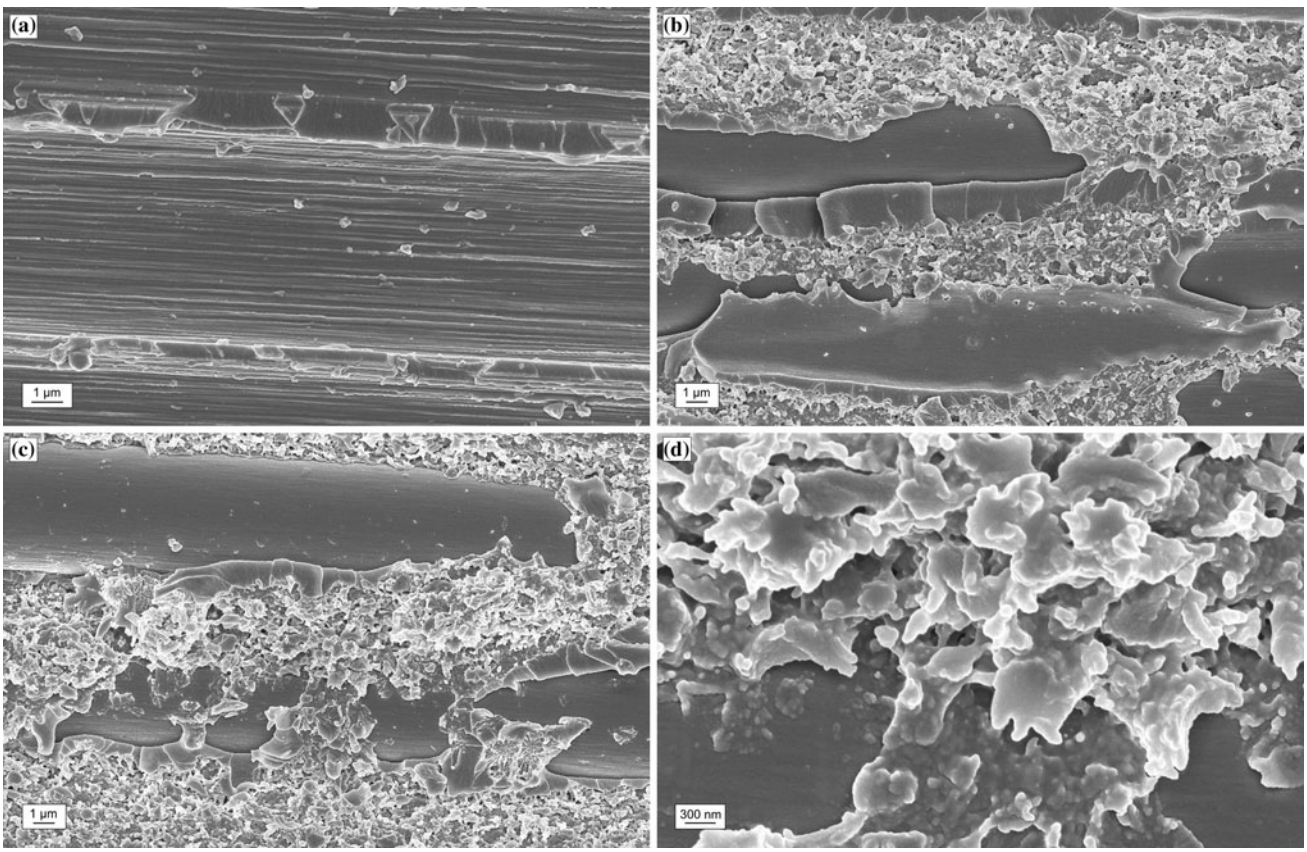

Fig. 13 Scanning electron micrograph of CFRP composites: (**a**) unmodified, (**b**) with 5 wt% E21, (**c**) with 10 wt% E21 and (**d**) high magnification of 10 wt% E21 (Crack propagation direction *right* to *left*)

test and on the fracture surfaces, although this is somewhat limited due to the woven nature of the fabrics.

When the epoxy matrix was modified with E21 SBM (see Fig. 13b-d), a much rougher fracture surface was observed with very few fibres visible, suggesting that a cohesive failure through the matrix had occurred. The microstructure was also slightly different from the bulk material in that the co-continuous structure was more evident. This can be explained by the space constraint of the tightly packed fibres which impedes the mobility of the SBM, and hence the SBM phase separates as a co-continuous structure.

There was also a lack of fibre bridging observed on the fracture surfaces, which is reflected in the relatively small R-curves described in the previous section. This reduction in fibre bridging was also noticeable during testing. The main toughening mechanisms can be identified from the fracture surfaces as debonding and plastic void growth around the SBM structure of the modified matrices, similar to the findings from the bulk material. However, any improvements in the matrix fracture energy could not be translated fully to the composite fracture energy because the plastic zone size is restricted by the relatively small inter-fibre distances as explained previously.

Conclusions

An anhydride-cured epoxy polymer was modified using two poly(styrene)-*b*-1,4-poly(butadiene)-*b*-poly(methyl methacrylate) (SBM) block copolymers supplied by Arkema, France. The E21 SBM contained more PB than the E41 copolymer and had a higher molecular weight. The microstructure, fracture properties and toughening mechanisms were identified. The E21 phase separated into spherical micelles, which became increasingly interconnected into a network as the concentration of modifier was increased. The addition of $\leq$7.5 wt% of E41 produced well dispersed 'raspberry'-like SBM particles with a PS core covered with PB particles in the epoxy matrix. Above 10 wt% of E41, partial phase inversion was observed, with SBM rich regions containing epoxy particles and epoxy-rich regions containing SBM particles.

The glass transition temperature of 157 °C was unaffected by the addition of E21 SBM, but the tensile modulus decreased, as expected when incorporating a relatively softer material into epoxy. The fracture energy, G_{IC}, was increased linearly to a maximum of 511 J/m^2 by the addition of 15 wt% E21 SBM. The main toughening mechanisms observed in this case were debonding of the SBM particles and subsequently plastic void growth. At loadings of $\leq$7.5 wt%, the E41 SBM modified epoxy polymers did not show significant toughness improvements. Here, debonding followed by some plastic void growth, and shear yielding were the observed toughening mechanisms. When partial phase inversion occurred, there was a significant increase in G_{IC}.

The toughness improvements shown in the E21 SBM modified epoxy polymers were not transferred into a CFRP composite system. The main toughening mechanisms for a fibre composite; fibre bridging, fibre debonding and fibre pullout, were suppressed when the matrix was modified with E21 due to increased fibre–matrix adhesion. The crack tip deformation zone was also restricted by the tightly packed fibres at higher SBM contents such that the measured composite fracture energy reached a plateau.

Acknowledgements The authors gratefully acknowledge the award of a PhD scholarship for Mr. H.M. Chong from the Department of Mechanical Engineering at Imperial College London. The authors would like to thank Evonik Hanse (Dr. S. Sprenger) and Arkema (Dr. T. Fine) for the supply of materials. Some of the equipment used was provided by Dr. A.C. Taylor's Royal Society Mercer Junior Award for Innovation.

References

1. Giannakopoulos G, Masania K, Taylor AC (2011) J Mater Sci 46(2):327. doi:10.1007/s10853-010-4816-6
2. Bagheri R, Pearson RA (1996) Polymer 37(20):4529. doi:10.1016/0032-3861(96)00295-9
3. Kinloch AJ, Shaw SJ, Tod DA, Hunston DL (1983) Polymer 24(October):1341. doi:10.1016/0032-3861(83)90070-8
4. Pearson RA, Yee AF (1986) J Mater Sci 21(7):2475. doi:10.1007/BF01114294
5. Cardwell BJ, Yee AF (1998) J Mater Sci 33(22):5473. doi:10.1023/A:1004427123388
6. White KL, Sue HJ (2011) Polym Eng Sci 51(11):2245. doi:10.1002/pen.21996
7. Bucknall CB, Partridge IK (1983) Polymer 24(5):639. doi:10.1016/0032-3861(83)90120-9
8. Kinloch AJ, Yuen ML, Jenkins SD (1994) J Mater Sci 29(14):3781. doi:10.1007/BF00357349
9. Hsieh TH, Kinloch AJ, Masania K, Taylor AC, Sprenger S (2010) Polymer 51(26):6284. doi:10.1016/j.polymer.2010.10.048
10. Johnsen BB, Kinloch AJ, Mohammed RD, Taylor AC, Sprenger S (2007) Polymer 48(2):530. doi:10.1016/j.polymer.2006.11.038
11. Mallick PK, Broutman LJ (1975) Mater Sci Eng 18(1):63. doi:10.1016/0025-5416(75)90073-7
12. Kawaguchi T, Pearson RA (2003) Polymer 44(15):4239. doi:10.1016/S0032-3861(03)00372-0
13. Hsieh TH, Kinloch AJ, Taylor AC, Kinloch IA (2011) J Mater Sci 46(12):7525. doi:10.1007/s10853-011-5724-0
14. Gojny FH, Wichmann MHG, Fiedler B, Schulte K (2005) Compos Sci Tech 65(15–16):2300. doi:10.1016/j.compscitech.2005.04.021
15. Park S-J, Jin F-L, Lee C (2005) Mater Sci Eng A 402(1–2):335

16. Brown EN, Sottos NR, White SR (2002) Exp Mech 42(4):372. doi:10.1007/BF02412141
17. Azimi HR, Pearson RA, Hertzberg RW (1995) J Appl Polymer Sci 58(2):449. doi:10.1002/app.1995.070580223
18. Manjunatha CM, Taylor AC, Kinloch AJ, Sprenger S (2009) J Mater Sci 44(1):342. doi:10.1007/s10853-008-3092-1
19. Hsieh TH, Kinloch AJ, Taylor AC, Sprenger S (2011) J Appl Polymer Sci 119(4):2135. doi:10.1002/app.32937
20. Hunston DL, Moulton RJ, Johnston NJ, Bascom WD (1987) In: Johnston NJ (ed) Toughened Composites. ASTM, Philadelphia, p 74
21. Fine T, Pascault J-P (2006) Macromol Symp 245–246(1):375. doi:10.1002/masy.200651352
22. Dean JM, Grubbs RB, Saad W, Cook RF, Bates FS (2003) J Polym Sci B 41(20):2444. doi:10.1002/polb.10595
23. Dean JM, Lipic PM, Grubbs RB, Cook RF, Bates FS (2001) J Polym Sci B 39(23):2996. doi:10.1002/polb.10062
24. Gerard P, Boupat NP, Fine T, Gervat L, Pascault J-P (2007) Macromol Symp 256:55. doi:10.1002/masy.200751006
25. Hydro RM, Pearson RA (2007) J Polym Sci Part B 45(12):1470. doi:10.1002/polb.21166
26. Ritzenthaler S, Court F, Girard-Reydet E, Leibler L, Pascault JP (2003) Macromolecules 36(1):118. doi:10.1021/ma0211075
27. Rebizant V, Abetz V, Tournilhac F, Court F, Leibler L (2003) Macromolecules 36(26):9889. doi:10.1021/ma0347565
28. Ritzenthaler S, Court F, David L, Girard-Reydet E, Leibler L, Pascault JP (2002) Macromolecules 35(16):6245. doi:10.1021/ma0121868
29. Thio YS, Wu JX, Bates FS (2006) Macromolecules 39(21):7187. doi:10.1021/ma052731v
30. Larrañaga M, Gabilondo N, Kortaberria G, Serrano E, Remiro P, Riccardi CC, Mondragon I (2005) Polymer 46(18):7082. doi:10.1016/j.polymer.2005.05.102
31. Thio YS, Wu JX, Bates FS (2009) J Polym Sci B 47(11):1125. doi:10.1002/polb.21707
32. Technical Data Sheet-Nanostrength for Epoxies (2011). Arkema, Colombes
33. XC305 Data Sheet (2012). Gurit, Newport
34. Hsieh TH, Kinloch AJ, Masania K, Sohn Lee J, Taylor AC, Sprenger S (2010) J Mater Sci 45(5):1193. doi:10.1007/s10853-009-4064-9
35. BS-EN-ISO-527-1 (1996) Plastics—Determination of Tensile Properties—Part 1: General Principles. BSI, London
36. Williams JG, Ford H (1964) J Mech Eng Sci 6(4):405
37. BS-EN-ISO-14125 (1998) Fibre-reinforced plastic composites—determination of flexural properties. BSI, London
38. BS-EN-ISO-14130 (1998) Fibre-reinforced plastic composites. Determination of apparent interlaminar shear strength by short-beam method. BSI, London
39. ASTM-D5045-99 (1999) Standard Test Methods for Plane-Strain Fracture Toughness and Strain Energy Release Rate of Plastic Materials. American Society for Testing and Materials, West Conshohocken
40. BS-7991 (2001) Determination of the mode I adhesive fracture energy, G_{IC}, of structural adhesives using the double cantilever beam (DCB) and tapered double cantilever beam (TDCB) specimens. BSI, London
41. Mimura K, Ito H, Kujioka H (2000) Polymer 41(12):4451. doi:10.1016/S0032-3861(99)00700-4
42. Biolley N, Pascal T, Sillion B (1994) Polymer 35(3):558
43. Cho JB, Hwang JW, Cho K, An JH, Park CE (1993) Polymer 34(23):4832. doi:10.1016/0032-3861(93)90005-U
44. Sultan JN, McGarry FJ (1973) Polym Eng Sci 13(1):29. doi:10.1002/pen.760130105
45. Bowden PB (1973) In: Haward RN (ed) The Physics of Glassy Polymers, 1st edn. Applied Science Publishers, London, p 279
46. Chen J, Taylor AC (2012) J Mater Sci 47(11):4546. doi:10.1007/s10853-012-6313-6
47. Thompson ZJ, Hillmyer MA, Liu J, Sue HJ, Dettloff M, Bates FS (2009) Macromolecules 42(7):2333. doi:10.1021/ma900061b
48. Liu J, Sue HJ, Thompson ZJ, Bates FS, Dettloff M, Jacob G, Verghese N, Pham H (2009) Polymer 50(19):4683. doi:10.1016/j.polymer.2009.05.006
49. Andrews EH (1968) Fracture in Polymers, 1st edn. Oliver & Boyd, Edinburgh
50. Mohammed RD (2007) Material properties and fracture mechanisms of epoxy nano-composites. PhD Thesis, Imperial College of Science, Technology & Medicine, London
51. Marissen R, Brouwer HR (1999) Compos Sci Tech 59(3):327. doi:10.1016/s0266-3538(98)00071-2
52. Irwin GR (1964) Appl Mater Res 3(2):65
53. Bradley WL (1989) Key Eng Mater 37:161
54. Hull D (1981) An Introduction to Composite Materials. Cambridge Solid State Science Series, 1 edn. Cambridge University Press, Cambridge
55. Quaresimin M, Varley RJ (2008) Compos Sci Technol 68(3–4):718. doi:10.1016/j.compscitech.2007.09.005